https://doi.org/10.1093/plcell/koad255 THE PLANT CELL 2024: 36: 158–173

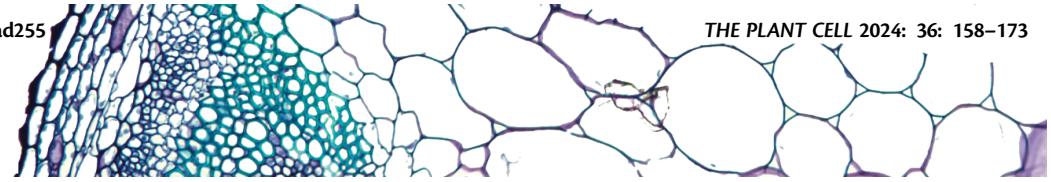

Research Article

Transcriptional activation by WRKY23 and derepression by removal of bHLH041 coordinately establish callus pluripotency in *Arabidopsis* regeneration

Chongyi Xu [1], Pengjie Chang [1,2], Shiqi Guo [1,2], Xiaona Yang [1,2], Xinchun Liu [1,2], Baofeng Sui [1,2], Dongxue Yu [1,2], Wei Xin [1,2] and Yuxin Hu [1,3,*]

1 Key Laboratory of Plant Molecular Physiology, Institute of Botany, Chinese Academy of Sciences, China National Botanical Garden, Beijing 100093, China
2 University of Chinese Academy of Sciences, Beijing 100049, China
3 National Center for Plant Gene Research, Beijing 100093, China

*Author for correspondence: huyuxin@ibcas.ac.cn
The author responsible for distribution of materials integral to the findings presented in this article in accordance with the policy described in the Instructions for Authors (https://academic.oup.com/plcell/pages/General-Instructions) is Yuxin Hu (huyuxin@ibcas.ac.cn).

Abstract

Induction of the pluripotent cell mass termed callus from detached organs or tissues is an initial step in typical in vitro plant regeneration, during which auxin-induced ectopic activation of root stem cell factors is required for subsequent de novo shoot regeneration. While *Arabidopsis* (*Arabidopsis thaliana*) AUXIN RESPONSE FACTOR 7 (ARF7) and ARF19 and their downstream transcription factors LATERAL ORGAN BOUNDARIES DOMAIN (LBD) are known to play key roles in directing callus formation, the molecules responsible for activation of root stem cell factors and thus establishment of callus pluripotency are unclear. Here, we identified *Arabidopsis* WRKY23 and BASIC HELIX-LOOP-HELIX 041 (bHLH041) as a transcriptional activator and repressor, respectively, of root stem cell factors during establishment of auxin-induced callus pluripotency. We show that auxin-induced WRKY23 downstream of ARF7 and ARF19 directly activates the transcription of *PLETHORA 3* (*PLT3*) and *PLT7* and thus that of the downstream genes *PLT1*, *PLT2*, and *WUSCHEL-RELATED HOMEOBOX 5* (*WOX5*), while LBD-induced removal of bHLH041 derepresses the transcription of *PLT1*, *PLT2*, and *WOX5*. We provide evidence that transcriptional activation by WRKY23 and loss of bHLH041-imposed repression act synergistically in conferring shoot-regenerating capability on callus cells. Our findings thus disclose a transcriptional mechanism underlying auxin-induced cellular reprogramming, which, together with previous studies, outlines the molecular framework of auxin-induced pluripotent callus formation for in vitro plant regeneration programs.

Introduction

A well-known feature of plant somatic cells is their remarkable capacity to regenerate a new organ or an entire plant under in vitro culture conditions (Birnbaum and Sanchez Alvarado 2008; Sugimoto et al. 2010; Sugimoto et al. 2011), during which the phytohormones auxin and cytokinin play a key role in determining cell fate transitions and regeneration programs (Skoog and Miller 1957; Duclercq et al. 2011; Ikeuchi et al. 2013). A typical in vitro plant regeneration generally starts with the induction of a pluripotent cell mass named callus from detached organs or tissues on auxin-rich callus-inducing medium (CIM); the subsequent incubation of newly formed calli on shoot-inducing medium (SIM) or root-inducing medium (RIM) with different ratios of auxin and cytokinin leads to the de novo production of shoots or roots, respectively (Skoog and Miller 1957; Valvekens et al.

Received May 10, 2023. Accepted September 13, 2023. Advance access publication October 6, 2023

IN A NUTSHELL

Background: Plant cells retain a remarkable capacity to regenerate new organs or entire individuals in the real world and under tissue culture conditions. A well-established in vitro plant regeneration procedure applicable for transgenic and biotechnological uses generally starts with the induction of pluripotent callus cells, which is required for subsequent de novo shoot or root regeneration. Recent studies in *Arabidopsis* (*Arabidopsis thaliana*) have revealed that auxin-induced ectopic activation of root stem cell factors within callus cells establishes the shoot-regenerating capability, and some auxin-signaling components involved in root development, such as AUXIN RESPONSE FACTOR (ARFs) and their downstream transcription factors LATERAL ORGAN BOUNDARIES DOMAIN (LBD), play critical roles in directing callus formation. However, the molecular link between these auxin-signaling components and activation of root stem cell factors during callus induction is missing.

Question: What are the factors responsible for activation of root stem cell factors to establish callus pluripotency in *Arabidopsis* for in vitro regeneration?

Findings: We identified the *Arabidopsis* transcription factors WRKY23 and bHLH041 as a transcriptional activator and repressor, respectively, of the expression of root stem cell genes during auxin-induced callus formation. Genetic and molecular evidence revealed that auxin-induced WRKY23 downstream of ARF7 and ARF19 directly activates the transcription of *PLETHORA 3* (*PLT3*) and *PLT7* and the downstream target genes of their encoded proteins *PLT1*, *PLT2*, and *WUSCHEL-RELATED HOMEOBOX 5* (*WOX5*), while LBD induces the removal of bHLH041, alleviating the transcriptional repression of *PLT1*, *PLT2*, and *WOX5*. We also demonstrated that two transcriptional pathways synergize the shoot-regenerating capability of callus cells. These findings elucidate the transcriptional mechanism underlying callus pluripotency establishment, which links auxin signaling and cellular reprogramming during in vitro plant regeneration programs.

Next steps: It will be worth identifying the orthologs of WRKY23 and bHLH041 in crops and economically important plants and exploring whether such regulatory mechanisms are conserved, which would potentially boost regeneration-based transgene and gene editing in these species.

1988; Che et al. 2002). Thus, auxin-induced callus formation has long been considered to reflect the mitotic activities of some differentiated cells that are reactivated, after which somatic cells are reprogrammed into pluripotent callus cells, which are required for subsequent de novo regeneration programs (Che et al. 2007; Gordon et al. 2007; Atta et al. 2009; Kareem et al. 2015).

Recent studies have begun to uncover the molecular characteristics of callus and regulation of auxin-induced callus formation during in vitro plant regeneration. In *Arabidopsis* (*Arabidopsis thaliana*), auxin-induced callus formation in multiple organs occurs from the pericycle or pericycle-like cells by a root developmental program; the root stem cell regulators, such as WUSCHEL-RELATED HOMEOBOX 5 (WOX5), PLETHORA 1 (PLT1), PLT2, SHORT-ROOT (SHR), and SCARECROW (SCR), are ectopically activated in the forming callus (Atta et al. 2009; Sugimoto et al. 2010; Kareem et al. 2015; Radhakrishnan et al. 2018). Consistent with this observation, several auxin-signaling components INDOLE-3-ACETIC ACID INDUCIBLE (IAA) and AUXIN RESPONSE FACTORs (ARFs) form modules involved in lateral root formation, such as IAA14/19–ARF7/19, playing a critical role in governing auxin-induced callus formation (Tian and Reed 1999; Fukaki et al. 2002; Tatematsu et al. 2004; Fukaki et al. 2005; Okushima et al. 2007; Uehara et al. 2008; Fan et al. 2012; Goh et al. 2012; Shang et al. 2016). Similarly, the auxin-inducible transcription factors LATERAL ORGAN BOUNDARIES DOMAIN (LBD), which act downstream of IAA14–ARF7/19 to control lateral root formation (Okushima et al. 2007; Lee et al. 2009; Lee et al. 2013; Lee et al. 2015; Lee, Kang, et al. 2017), are key factors in directing callus formation by forming a complex with BASIC LEUCINE ZIPPER 59 (bZIP59) (Fan et al. 2012; Xu, Cao, Xu, et al. 2018; Xu, Cao, Zhang, et al. 2018). Moreover, ARABIDOPSIS TRITHORAX-RELATED 2 (ATXR2) recruited by ARF7 and ARF19 can promote callus formation by activation of *LBD* gene expression (Lee, Park, and Seo 2017), while the calcium signaling module CALMODULIN–IQ-MOTIF CONTAINING PROTEIN (CaM–IQM) regulates callus formation by destabilizing the interaction of IAA and ARF7/19 (Zhang et al. 2022). Notably, the ectopic activation of root stem cell factors including PLTs and WOX5, which are considered to be root pluripotent transcription factors (Wang et al. 2022), represents the acquisition of cellular pluripotency or shoot-regenerating capability in the forming callus cells (Sugimoto et al. 2010; Kareem et al. 2015). Indeed, HISTONE ACETYLTRANSFERASE 1 (HAG1) promotes regeneration competence of callus cells by upregulation of several root-meristem regulator genes including *WOX5*, *PLT1*, and *PLT2* (Kim et al. 2018), while the interaction of WOX5 with PLT1 and PLT2 to promote *TRYPTOPHAN AMINOTRANSFERASE OF ARABIDOPSIS 1* (*TAA1*) expression is critical for maintenance of pluripotency in the middle layer of callus cells (Zhai and Xu 2021; Zhai et al. 2023).

Importantly, PLT3, PLT5, and PLT7 function redundantly in conferring shoot-regenerating competence of callus cells by activating *PLT1* and *PLT2* expression, as calli derived from the explants of the *plt3 plt5 plt7* triple mutant are largely defective in shoot-regenerating capability (Kareem et al. 2015). Intriguingly, the WOX11–LBD16 module promotes the acquisition of callus pluripotency by affecting transcription of *PLT1* and *PLT2* but not of *PLT3* or *PLT7* (Liu et al. 2018), suggesting that at least two molecular pathways are involved in activating root stem cell regulators and thus establishing cellular pluripotency (Sugiyama 2018). However, the molecules responsible for activation of these root pluripotent factors during auxin-induced callus formation are unclear.

Here, we reported that the *Arabidopsis* transcription factors WRKY23 and BASIC HELIX-LOOP-HELIX 041 (bHLH041) act as a transcriptional activator and repressor, respectively, downstream of IAA–ARFs to coordinate the activation of root stem cell genes during callus induction. We show that WRKY23, encoded by auxin-induced *WRKY23* downstream of ARF7 and ARF19 directly activates the transcription of *PLT3* and *PLT7*, whose encoding proteins in turn activate the transcription of the downstream genes *PLT1*, *PLT2*, and *WOX5*, and that LBD-induced removal of bHLH041 alleviates the transcriptional repression of *PLT1*, *PLT2*, and *WOX5*. We also provide evidence that transcriptional activation by WRKY23 and derepression by bHLH041 synergize the shoot-regenerating capability of callus cells. These findings uncover a transcriptional mechanism underlying cellular pluripotency establishment during in vitro plant regeneration programs.

Results

WRKY23 and bHLH041 are respectively accumulated and abolished in forming callus

As previous studies have suggested that two molecular pathways are involved in activation of *PLT3* and *PLT7* and LBD-induced *PLT1* and *PLT2* transcription, respectively (Kareem et al. 2015; Liu et al. 2018; Sugiyama 2018), we wished to identify the transcription factors responsible for activation of these root stem cell genes during callus formation on CIM. To this end, we focused on genes whose expression patterns are correlated with those of *PLT3* and *PLT7* in a transcriptomic profiling of *Arabidopsis* explants on CIM and the potential LBD29-regulated genes whose transcript and/or protein accumulation are possibly associated with activation of *PLT1* and *PLT2*. In an *Arabidopsis* ATH1 GeneChip database of transcript levels from root explants incubated on CIM (Che et al. 2006), we noticed that the dynamics of *WRKY23*, which encodes a member of the plant-specific WRKY family of transcription factors (Prát et al. 2018), was similar to those of *PLT3* and *PLT7* (Supplemental Fig. S1A). Reverse transcription quantitative PCR (RT-qPCR) analysis showed that *WRKY23* transcript levels are elevated (close to 20-fold after 5 d) after incubation of seedlings on CIM (Fig. 1A). Next, we examined WRKY23 accumulation with transgenic *ProWRKY23:gWRKY23-GFP* seedlings harboring a transgene consisting of the *WRKY23* promoter driving the *WRKY23* genomic coding region cloned in-frame and upstream of the green fluorescent protein (*GFP*) sequence, when incubated on CIM. Although we detected WRKY23-GFP in the nuclei of pericycle or pericycle-like cells and other cells, its abundance markedly increased in the callus cells forming from roots, hypocotyls, and cotyledons after seedlings were incubated on CIM (Fig. 1B; Supplemental Fig. S1B). Among the transcription factor genes potentially regulated by LBD29 (Xu, Cao, Xu, et al. 2018), the transcript abundance of *bHLH041*, which encodes a member of the bHLH family (Toledo-Ortiz et al. 2003), was rapidly induced by chemically induced LBD29 but dramatically declined afterward (Xu, Cao, Xu, et al. 2018) (Supplemental Fig. S1C). We confirmed by RT-qPCR analysis that *bHLH041* transcript levels are initially induced by incubation on CIM but decline later (Fig. 1A). Surprisingly, with the transgenic *ProbHLH041:bHLH041-GFP* seedlings, we observed that bHLH041 accumulates ubiquitously in the nuclei of all cells in roots, hypocotyls, and cotyledons; however, after seedlings were incubated on CIM, bHLH041 abundance gradually declined in these cells and bHLH041 completely disappeared in the forming callus (Fig. 1B; Supplemental Fig. S1D). Immunoblotting analysis confirmed that WRKY23 and bHLH041 abundance increases and declines by incubation on CIM, respectively (Fig. 1C). These observations suggest that WRKY23 and bHLH041 might participate in auxin-induced callus formation.

WRKY23 and bHLH041 respectively promote and inhibit callus formation and shoot regeneration

As WRKY23 has been reported to act downstream of ARF7 and ARF19 to regulate root development (Grunewald et al. 2012), we reasoned that WRKY23 might be involved in auxin-induced callus formation and possibly shoot regeneration. To test this idea, we generated 3 allelic mutants of *WRKY23*, namely *wrky23-3*, *wrky23-4*, and *wrky23-5*, by clustered regularly interspaced short palindromic repeat (CRISPR)/CRISPR-associated nuclease 9 (Cas9)-mediated gene editing (Supplemental Fig. S2A) and examined their callus-forming and shoot-regenerating phenotypes. When compared to wild type (WT), loss of WRKY23 function not only attenuated callus formation from cotyledon and root explants when incubated on CIM but also dampened shoot regeneration from the derived calli after incubation on SIM (Fig. 2A). Moreover, such callus-forming and shoot-regenerating defect in *wrky23-3* explants and derived callus could be rescued by introduction of the *ProWRKY23:gWRKY23-GFP* construct, confirming that these phenotypes can be attributed to the loss of WRKY23 (Fig. 2A). We also generated transgenic *35S:WRKY23* plants overexpressing *WRKY23* from the cauliflower mosaic (CaMV) 35S promoter and examined their callus-forming and shoot-regenerating phenotype. The overexpression of *WRKY23* promoted callus formation and shoot regeneration from cotyledon and root explants and their derived callus in a *WRKY23* transcript

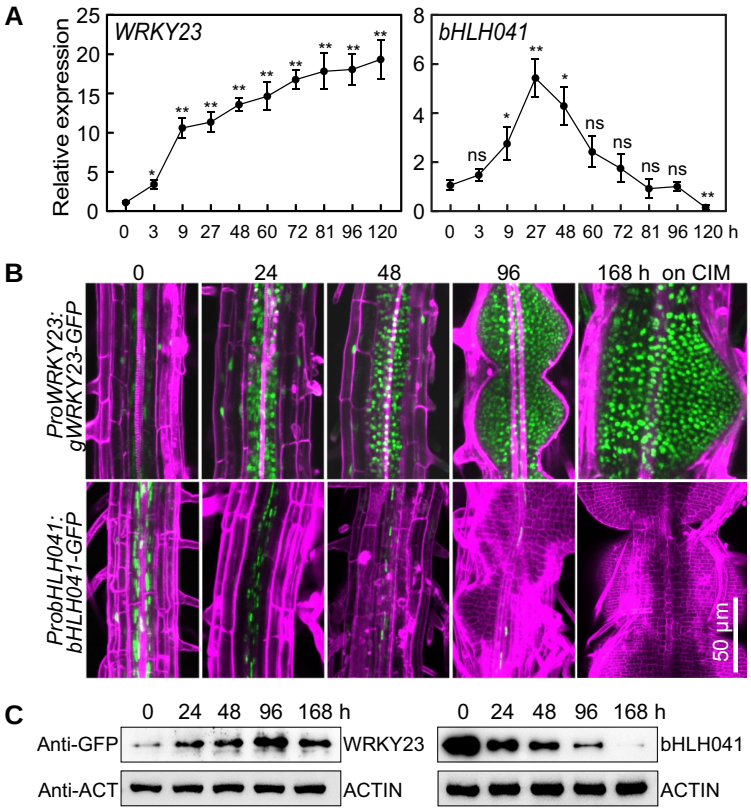

Figure 1. Accumulation of WRKY23 and bHLH041 during callus induction. **A)** Relative *WRKY23* and *bHLH041* transcript levels in response to CIM. Seven-day-old wild type (WT) seedlings incubated in liquid CIM for the indicated times were used for RNA isolation and RT-qPCR analysis. Data are shown as means ± SD ($n = 3$ biological replicates). *$P < 0.05$, **$P < 0.01$ by *t*-test. **B, C)** Accumulation of WRKY23 and bHLH041 during callus induction. Five-d-old transgenic seedlings carrying a *ProWRKY23:gWRKY23-GFP* or *ProbHLH041:bHLH041-GFP* transgene were incubated on CIM for the indicated times. GFP signals from the mature zone of primary roots were overlaid with signals stained with propidium iodide in **B)**, and the total proteins from seedlings were immunoblotted by anti-GFP and anti-ACTIN antibodies for 2 biological replicates in **C)**. Scale bar, 50 μm.

level-dependent manner (Fig. 2B; Supplemental Fig. S2B). These observations demonstrate that WRKY23 is a positive regulator of callus formation and shoot regeneration. In addition, *wrky23* and *35S:WRKY23* seedlings developed slightly shorter or longer primary roots with fewer or more lateral root initiates when compared to WT, respectively (Supplemental Fig. S2C), while their cotyledons were of comparable size among the 3 genotypes (Supplemental Fig. S2D).

To test whether bHLH041 participates in the regeneration program, we obtained a loss-of-function and a gain-of-function mutant of *bHLH041*, *bhlh041-1* (SAIL_330_F04), and *bhlh041-D* (SAIL_258_C53), in which a T-DNA was inserted in fourth exon or 5′ UTR of *bHLH041* and leads to the disruption or overexpression of *bHLH041*, respectively (Supplemental Fig. S3A). After incubation on CIM, the cotyledon and root explants of *bhlh041-1* displayed an enhanced callus-forming phenotype, whereas those of *bhlh041-D* had a callus-forming defect when compared to WT (Fig. 2C). We also observed a respective enhanced and dampened shoot regeneration phenotype in the calli derived from *bhlh041-1* and *bhlh041-D* after being incubated on SIM (Fig. 2C). Moreover, the enhanced callus-forming and shoot-regenerating phenotype of *bhlh041-1* was rescued by introduction of a transgene carrying the native *bHLH041* promoter driving *bHLH041* expression (Fig. 2C), and overexpression of *bHLH041* strongly inhibited the callus formation and shoot regeneration from explants and derived calli (Fig. 2D; Supplemental Fig. S3B). Collectively, we conclude that bHLH041 negatively regulates callus formation and shoot regeneration. In addition, we observed that disruption or overexpression of *bHLH041* resulted in an increase or decrease of lateral root numbers, respectively (Supplemental Fig. S3C). Notably, only dramatic overexpression of *bHLH041* (several hundred-fold higher than WT) had an effect on cotyledon development (Supplemental Fig. S3D).

WRKY23 and bHLH041 are involved in the regulation of root stem cell genes

As WRKY23 and bHLH041 affect both callus formation and shoot regeneration, we investigated whether they participate in the activation of root stem cell genes during callus induction. First, we monitored the transcript abundance of *WOX5*, *PLT*s, and *SHR* and in the WT, *wrky23-3*, *35S:WRKY23*, *bhlh041-1*, and *bhlh041-D* root explants incubated on CIM for 7 d. When compared to those in WT, the transcript levels

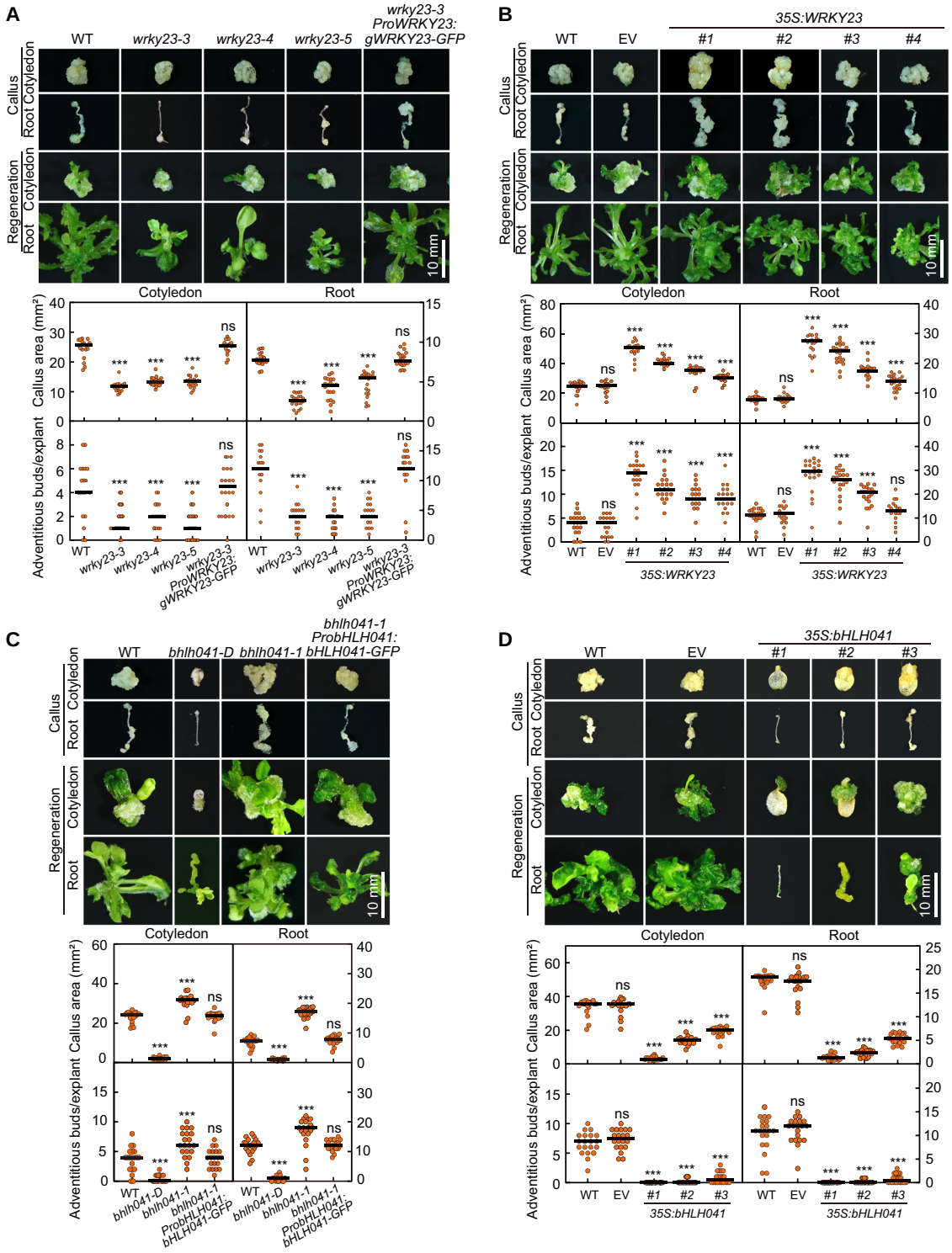

Figure 2. WRKY23 and bHLH041 regulate callus formation and shoot regeneration. **A)** Callus-forming and shoot-regenerating phenotypes of WT, *wrky23-3*, *wrky23-4*, *wrky23-5*, and *wrky23-3 ProWRKY23:gWRKY23-GFP* explants and derived calli. **B)** Callus-forming and shoot-regenerating phenotypes of WT, empty vector (EV), and *35S:WRKY23* explants and derived calli. Four independent *35S:WRKY23* transgenic lines named *#1*, *#2*, *#3*, and *#4* were examined. **C)** Callus-forming and shoot-regenerating phenotypes of WT, *bhlh041-D*, *bhlh041-1*, and *bhlh041-1 ProbHLH041:bHLH041-GFP* explants and derived calli. **D)** Callus-forming and shoot-regenerating phenotypes of WT, EV, and *35S:bHLH041* explants and derived calli. Three independent *35S:bHLH041* transgenic lines named *#1*, *#2*, and *#3* were examined. The cotyledon and root explants from 7-d-old seedlings were incubated on CIM for 21 d or for 7 d and subsequently on SIM for 14 d before being examined for callus formation and shoot regeneration, respectively. The callus area of each explant and the number of regenerating shoots from each callus were determined ($n = 20$ explants). Scale bars, 10 mm. Data are shown as means ± SD. $^{*}P < 0.05$, $^{**}P < 0.01$, and $^{***}P < 0.001$ by *t*-test.

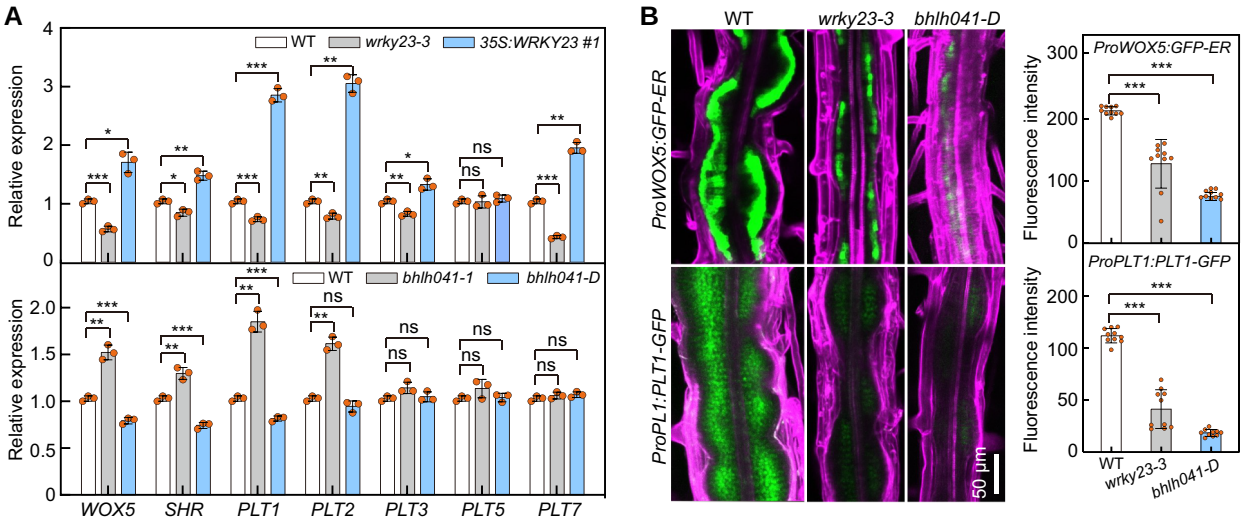

Figure 3. WRKY23 and bHLH041 are activator and repressor of root stem cell genes, respectively. **A)** Transcript abundance of root stem cell genes in root explants with forming callus from WT, *wrky23-3*, and *35S:WRKY23* (upper panel) and WT, *bhlh041-1*, and *bhlh041-D* (bottom panel). RT-qPCR analysis was performed with root explants incubated on CIM for 7 d ($n = 3$ biological replicates). **B)** Accumulation of *WOX5* and PLT1 in the callus-forming roots of WT, *wrky23-3*, and *bhlh041-D*. Five-d-old transgenic seedlings carrying a *ProWOX5:GFP-ER* or *ProPLT1:PLT1-YFP* transgene were incubated on CIM for 4 d, and GFP fluorescent signals were visualized and quantified at the mature zone of primary roots ($n = 10$ seedlings). The GFP signals were overlaid with the cells stained with propidium iodide. Scale bar, 50 μm. Data are shown as means ± SD. $^{*}P < 0.05$, $^{**}P < 0.01$, and $^{***}P < 0.001$ by *t*-test.

of *WOX5*, *SHR*, *PLT1*, *PLT2*, *PLT3*, and *PLT7* were lower in *wrky23-3* but higher in *35S:WRKY23* explants (Fig. 3A). By contrast, we observed elevated and decreased transcript levels for *WOX5*, *SHR*, *PLT1*, and *PLT2* in *bhlh041-1* and *bhlh041-D* explants, respectively (Fig. 3A). Next, we visualized the cellular accumulation of PLT1 and *WOX5*, two root stem cell markers ectopically activated within callus cells (Sugimoto et al. 2010), in *wrky23-3* and *bhlh041-D* plants harboring a *ProPLT1:PLT1-YFP* (yellow fluorescent protein) or *ProWOX5:GFP-ER* construct, respectively. We observed that disruption of *WRKY23* or overexpression of *bHLH041* leads to a drop in PLT1 accumulation and *WOX5* expression levels in the forming callus (Fig. 3B). These observations indicate that WRKY23 and bHLH041 are involved in the regulation of root stem cell genes and thus establishment of callus pluripotency. We also noticed that *PLT3* and *PLT7* transcript levels are only regulated by WRKY23 but not by bHLH041, suggesting that they might execute their roles via different pathways.

WRKY23 directly activates the transcription of *PLT3* and *PLT7*

Both WRKY23 and LBDs have been shown to act downstream of ARF7 and ARF19 to regulate lateral root development and/or callus formation (Grunewald et al. 2008; Fan et al. 2012; Grunewald et al. 2012; Xu, Cao, Zhang, et al. 2018). Consistent with the notion that ARF-mediated auxin signaling is mainly through auxin-induced degradation of their repressor IAAs but not by alteration of their abundances (Wang et al. 2005; Lavy and Estelle 2016; Powers et al. 2019), we determined that only the transcript levels of *ARF19* but not *ARF7* show a slight response to CIM (Supplemental Fig. S4A). To clarify the possible inter-regulation between *WRKY23* and *LBDs*, we first monitored the transcript levels of *WRKY23* in WT, *arf7 arf19*, and *lbd16-2 air1-2* (*anthocyanin-impaired response 1-2*, in which the *bZIP59* gene is disrupted) seedlings on CIM. Consistent with previous observations (Grunewald et al. 2012), induction of *WRKY23* by CIM was abolished in the *arf7 arf19* but not in the *lbd16-2 air1-2* mutant seedlings (Fig. 4A). Similarly, overexpression of *LBD16* or *LBD29* did not have a clear effect on *WRKY23* transcript levels (Supplemental Fig. S4B), supporting the notion that WRKY23 acts downstream of ARF7 and ARF19 but not of LBDs. Interestingly, we observed that overexpression of *WRKY23* results in higher transcript levels for *LBD16* and *LBD29* (Supplemental Fig. S4C), suggesting that WRKY23 has some degree of regulatory effect on *LBDs*. Furthermore, ectopic expression of *WRKY23* indeed partially rescued the callus-forming and shoot-regenerating defect observed in *arf7 arf19* explants and derived calli (Fig. 4B; Supplemental Fig. S5A). However, we failed to detect any binding activity of ARF7 toward the promoter region of *WRKY23* by chromatin immunoprecipitation-qPCR (ChIP-qPCR) assay performed with transgenic *ProARF7:ARF7-GFP* seedlings treated with CIM; we also observed no transcriptional activity of ARF7 toward a *ProWRKY23:LUC* (firefly luciferase gene) reporter construct in a transcriptional activation assay in *Arabidopsis* protoplasts (Supplemental Fig. S5, B to D). These observations further support the idea that *WRKY23* is an indirect target of ARF7 and ARF19 (Prát et al. 2018).

Since WRKY23 could promote the transcript levels of *PLT3* and *PLT7* as well as *PLT1* and *PLT2* (Fig. 3A) and as PLT3, PLT5, and PLT7 were shown to function redundantly in the transcriptional activation of *PLT1* and *PLT2* (Kareem et al.

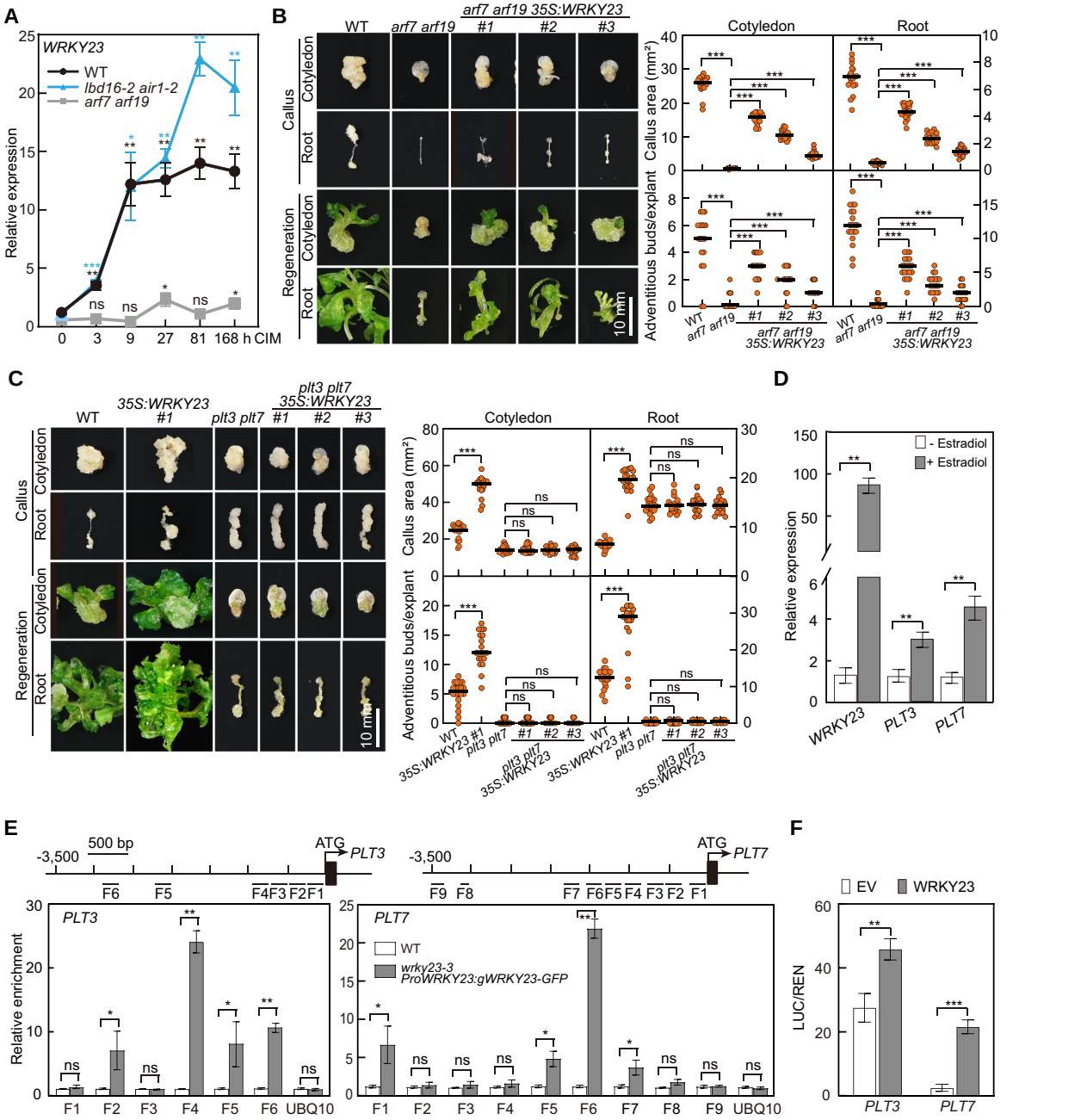

Figure 4. WRKY23 acts downstream of ARF7 and ARF19 and directly activates transcription of *PLT3* and *PLT7*. **A)** Relative *WRKY23* transcript levels in response to CIM in *arf7 arf19* and *lbd16-2 air1-2* seedlings. Seven-day-old seedlings were incubated in liquid CIM for the indicated times, and the relative expression level at 0 h was set to 1; data are shown as means ± SD ($n = 3$ biological replicates). **B)** Callus-forming and shoot-regenerating phenotypes of WT, *arf7 arf19*, and *arf7 arf19 35S:WRKY23* explants and derived calli ($n = 20$ explants). Scale bar, 10 mm. **C)** Callus-forming and shoot-regenerating phenotypes of WT, *35S:WRKY23*, *plt3 plt7*, and *plt3 plt7 35S:WRKY23* explants ($n = 20$ explants) and derived calli. Scale bar, 10 mm. Three independent transgenic lines of *arf7 arf19 35S:WRKY23* and *plt3 plt7 35S:WRKY23* named *#1*, *#2*, and *#3* were examined in **B)** and **C)**, respectively. **D)** Induction of *PLT3* and *PLT7* transcript levels by WRKY23. Five-d-old transgenic *ProXVE:WRKY23* seedlings were incubated in liquid B5 medium containing 10 μM 17-β-estradiol or DMSO (Mock) for 3 h, and relative expression levels are shown as means ± SD ($n = 3$ biological replicates). **E)** ChIP-qPCR assay showing the WRKY23 binding activity to the *PLT3* and *PLT7* promoters. ChIP-qPCR was performed with 10-d-old WT and *wrky23-3 ProWRKY23:gWRKY23-GFP* seedlings incubated in liquid CIM for 48 h with an anti-GFP antibody, and the enrichment of *PLT3* or *PLT7* promoter fragments F-1 to F-9 are indicated. A fragment of the *UBQ10* promoter was used as a negative control. Data are shown as means ± SD ($n = 3$ biological replicates). **F)** Transcriptional activation of *PLT3* and *PLT7* by WRKY23. The activity of the *ProPLT3:LUC* or *ProPLT7:LUC* reporter was determined in *Arabidopsis* protoplasts cotransfected with an empty vector (EV), or *35S:Ω:WRKY23-GFP* (WRKY23) construct, together with each LUC reporter. Data are shown as means of the original LUC/REN ratios × 100 ± SD ($n = 3$ biological replicates). $^*P < 0.05$, $^{**}P < 0.01$, and $^{***}P < 0.001$ by *t*-test.

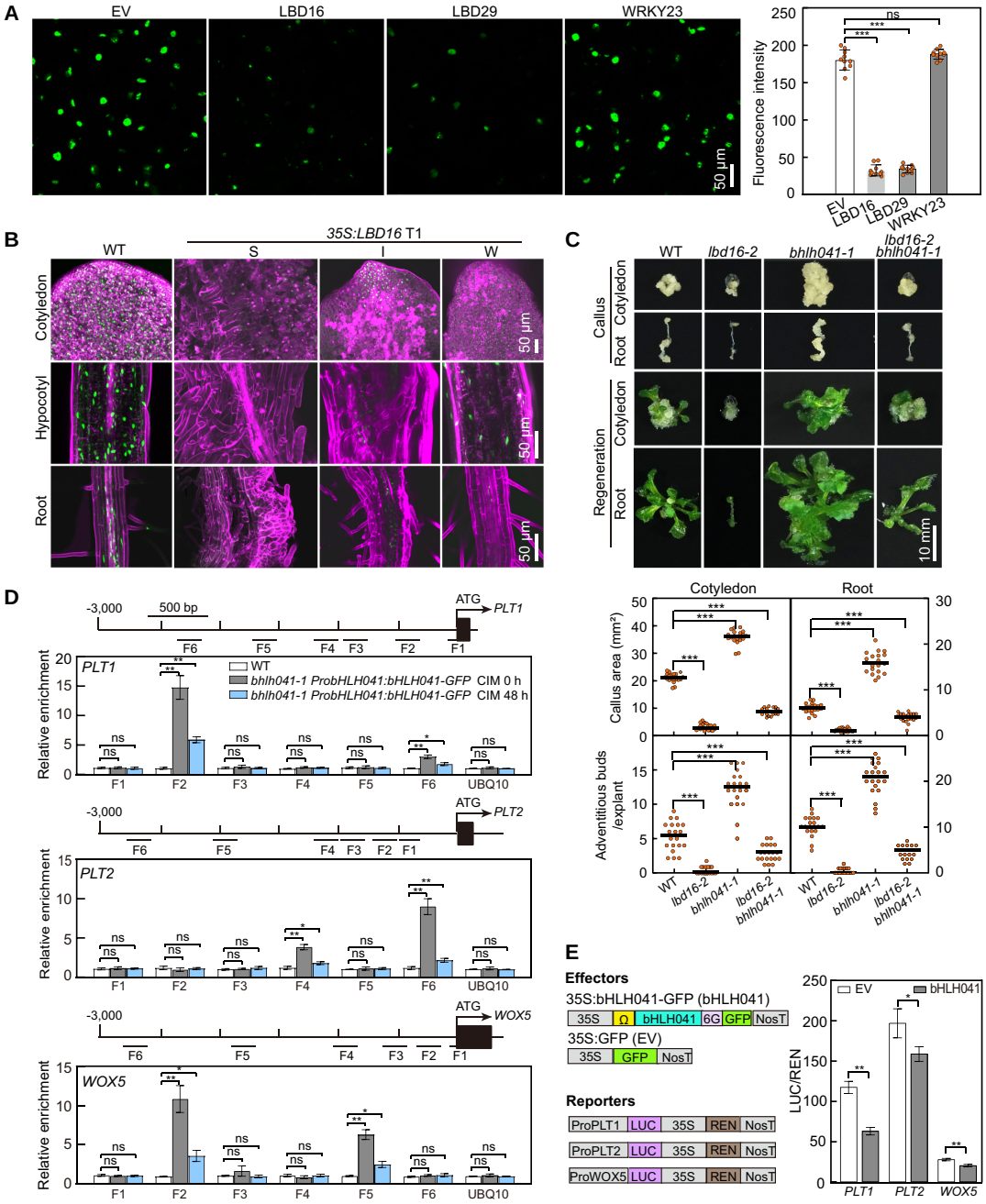

Figure 5. LBD induces the removal of bHLH041 to alleviate bHLH041-mediated repression of *PLT1*, *PLT2*, and *WOX5* transcription. **A**, **B**) Over-accumulation of LBD16 or LBD29 induces the disappearance of bHLH041. The fluorescent signals of bHLH041-GFP were visualized in *N. benthamiana* leaves transiently coexpressing *bHLH041-GFP* with an empty vector (EV), *LBD16-FLAG* (LBD16), *LBD29-FLAG* (LBD29), or *WRKY23-FLAG* (WRKY23) for 4 d ($n = 10$ leaves) **A)** and in transgenic *Arabidopsis ProbHLH041:bHLH041-GFP* seedlings harboring a *35S:LBD16* construct with a strong (S), intermediate (I), or weak (W) autonomous callus-forming phenotype **B)**. Scale bars, 50 μm. **C)** Callus-forming and shoot-regenerating phenotypes of WT, *lbd16-2*, *bhlh041-1*, and *lbd16-2 bhlh041-1*, explants and derived calli ($n = 20$ explants). Scale bar, 10 mm. **D)** ChIP-qPCR assay of bHLH041 binding activity to the *PLT1*, *PLT2*, and *WOX5* promoters. Ten-day-old WT and *bhlh041-1 ProbHLH041:bHLH041-GFP* seedlings incubated in liquid CIM for 0 and 48 h were assayed by ChIP-qPCR with anti-GFP antibody, and enrichments of the amplified F-1 to F-6 from *PLT1*, *PLT2*, or *WOX5* promoters are indicated. A fragment of the *UBQ10* promoter was used as a negative control. Data are shown as means ± SD ($n = 3$ biological replicates). **E)** bHLH041 inhibits *PLT1*, *PLT2*, and *WOX5* transcription. Left, diagrams of effector and reporter constructs used. Ω, translational enhancer. *Arabidopsis* protoplasts were cotransfected with the *LUC* reporter *PLT1:LUC*, *PLT2:LUC*, or *WOX5:LUC* with an empty vector (EV) or *35S:Ω:bHLH041-GFP* construct (bHLH041) and incubated in CIM for 16 h. LUC and REN activities were determined and shown as means of original LUC/REN ratios × 100 ± SD ($n = 3$ biological replicates). *$P < 0.05$, **$P < 0.01$, and ***$P < 0.001$ by *t*-test.

2015), we tested whether *PLT3* and/or *PLT7* are targets of WRKY23. When *WRKY23* was overexpressed in the *plt3 plt7* double mutant, whose callus exhibits a defect in shoot regeneration (Kareem et al. 2015), the enhanced shoot-regeneration capacity observed in the *35S:WRKY23* calli was abolished (Fig. 4C; Supplemental Fig. S5E). Next, we generated transgenic plants carrying a chemically inducible *OLexA-46* (also known as *G1090:XVE*) promoter driving *WRKY23* expression (*ProXVE:WRKY23*) (Zuo et al. 2000) and observed that treatment with the inducer 17-β-estradiol leads to higher transcript levels for *PLT3* and *PLT7* (Fig. 4D). Furthermore, we performed a ChIP-qPCR assay with transgenic *wrky23-3 ProWRKY23:gWRKY23-GFP* seedlings incubated in liquid CIM, which revealed that WRKY23 can bind to the promoter regions of *PLT3* and *PLT7* but not to the *PLT1*, *PLT2*, and *WOX5* promoters (Fig. 4E; Supplemental Fig. S5F). A transcriptional activation assay carried out in *Arabidopsis* protoplasts using *ProPLT3:LUC* and *ProPLT7:LUC* reporter constructs clearly showed that transiently expressing *WRKY23* leads to a higher relative LUC activity derived from the 2 reporter constructs (Fig. 4F; Supplemental Fig. S5C). Collectively, we conclude that following the induction of its transcription by auxin, WRKY23 downstream of ARF7 and ARF19 directly activates *PLT3* and *PLT7* transcription.

LBD-induced bHLH041 disappearance alleviates the transcriptional repression of *PLT1*, *PLT2*, and *WOX5*

Since CIM-induced disappearance of bHLH041 results in the activation of *PLT1*, *PLT2*, and *WOX5*, which is suggested to contribute to LBD-triggered acquisition of callus pluripotency (Liu et al. 2018), we reasoned that bHLH041 might act downstream of the ARF7/19–LBD module to repress the transcription of *PLT1*, *PLT2*, and *WOX5*. Indeed, we determined that disruption of *ARF7* and *ARF19* completely blocks the CIM-induced disappearance of bHLH041 in the pericycle cells of root explants, strengthening the idea that bHLH041 is downstream of ARF7 and ARF19 (Supplemental Fig. S6A). Next, we investigated whether disappearance of bHLH041 is related to LBD accumulation. To this end, we coexpressed *bHLH041-GFP* with *LBD16-FLAG*, *LBD29-FLAG*, or *WRKY23-FLAG* in *Nicotiana benthamiana* leaves; we observed much lower GFP fluorescent signals for bHLH041-GFP in the presence of LBD16 or LBD29 but not WRKY23 (Fig. 5A). In agreement, the overexpression of *LBD16* or *LBD29* in *ProbHLH041:bHLH041-GFP* plants largely abolished bHLH041 accumulation in multiple organs (Fig. 5B; Supplemental Fig. S6B), demonstrating that LBD accumulation leads to the disappearance of bHLH041. Moreover, we generated the *lbd16-2 bhlh041-1* double mutant: we determined that the callus-forming and shoot-regenerating defect of *lbd16-2* is partially rescued by the introduction of the *bhlh041-1* mutation (Fig. 5C), supporting the notion that bHLH041 is downstream of LBDs in controlling callus formation and regeneration capacity.

To further test whether the *PLT1*, *PLT2*, and *WOX5* are targeted by bHLH041 during auxin-induced callus formation, we performed ChIP-qPCR analysis with *bhlh041-1 ProbHLH041:bHLH041-GFP* seedlings before and after incubation on CIM. We observed that bHLH041 can bind to specific regions of the *PLT1*, *PLT2*, and *WOX5* promoters, with the binding enrichment decreasing after seedlings were incubated on CIM (Fig. 5D). We also conducted a transcriptional activity assay in *Arabidopsis* protoplasts incubated in CIM, using *ProPLT1:LUC*, *ProPLT2:LUC*, and *ProWOX5:LUC* reporter constructs and *35S:bHLH041* as effector construct. Cotransfecting each LUC reporter with the *35S:bHLH041* effector construct resulted in lower relative LUC activity from all reporters (Fig. 5E). Taken together, we conclude that LBD-induced disappearance of bHLH041 derepresses the transcription of *PLT1*, *PLT2*, and *WOX5*, thus coordinating the establishment of callus pluripotency.

WRKY23 and bHLH041 synergize shoot-regenerating capacity of callus

Since both the WRKY23–PLT3/7 and LBD–bHLH041 modules participate in the activation of *PLT1*, *PLT2*, and *WOX5*, we postulated that two modules synergize the shoot-regeneration capability of callus cells. To test this hypothesis, we crossed the *35S:WRKY23* line to the *bhlh041-1* mutant and obtained *bhlh041-1 35S:WRKY23* plants and examined the callus-forming phenotype of their root explants and the shoot-regenerating capability of their derived calli. When compared to those of *35S:WRKY23* and *bhlh041-1*, the callus-forming and shoot-forming phenotypes were additive in the *bhlh041-1 35S:WRKY23* explants and derived calli (Fig. 6A). Consistent with this finding, the transcript levels of *WOX5*, *SHR*, *PLT1*, and *PLT2* in the *bhlh041-1 35S:WRKY23* root explants were higher than those of *35S:WRKY23* or *bhlh041-1* root explants after being incubated on CIM (Fig. 6B). Next, we generated the *bhlh041-D wrky23-3* double mutant and discovered that both the callus-forming and shoot-regenerating defects in the *wrky23-3* root explants and derived calli are further enhanced by introduction of *bhlh041-D* (Fig. 6C) and that the transcript levels of *WOX5*, *PLT1*, *PLT2*, and *SHR* in *bhlh041-D wrky23-3* are substantially lower than in the *wrky23-3* or *bhlh041-D* root explants incubated on CIM (Fig. 6D). These observations demonstrate that transcriptional activation of WRKY23 and derepression by removal of bHLH041 synergistically establish callus pluripotency during in vitro regeneration programs.

Discussion

Although accumulating evidence demonstrates that several auxin-signaling components including IAA-ARFs and LBDs are critical regulators of auxin-induced callus formation (Fan et al. 2012; Shang et al. 2016; Xu, Cao, Zhang, et al. 2018) and that ectopic activation of root stem cell factors including PLTs and WOX5 are required for de novo shoot or root regeneration (Che et al. 2007; Atta et al. 2009; Sugimoto et al. 2010; Kareem et al. 2015), the molecular links

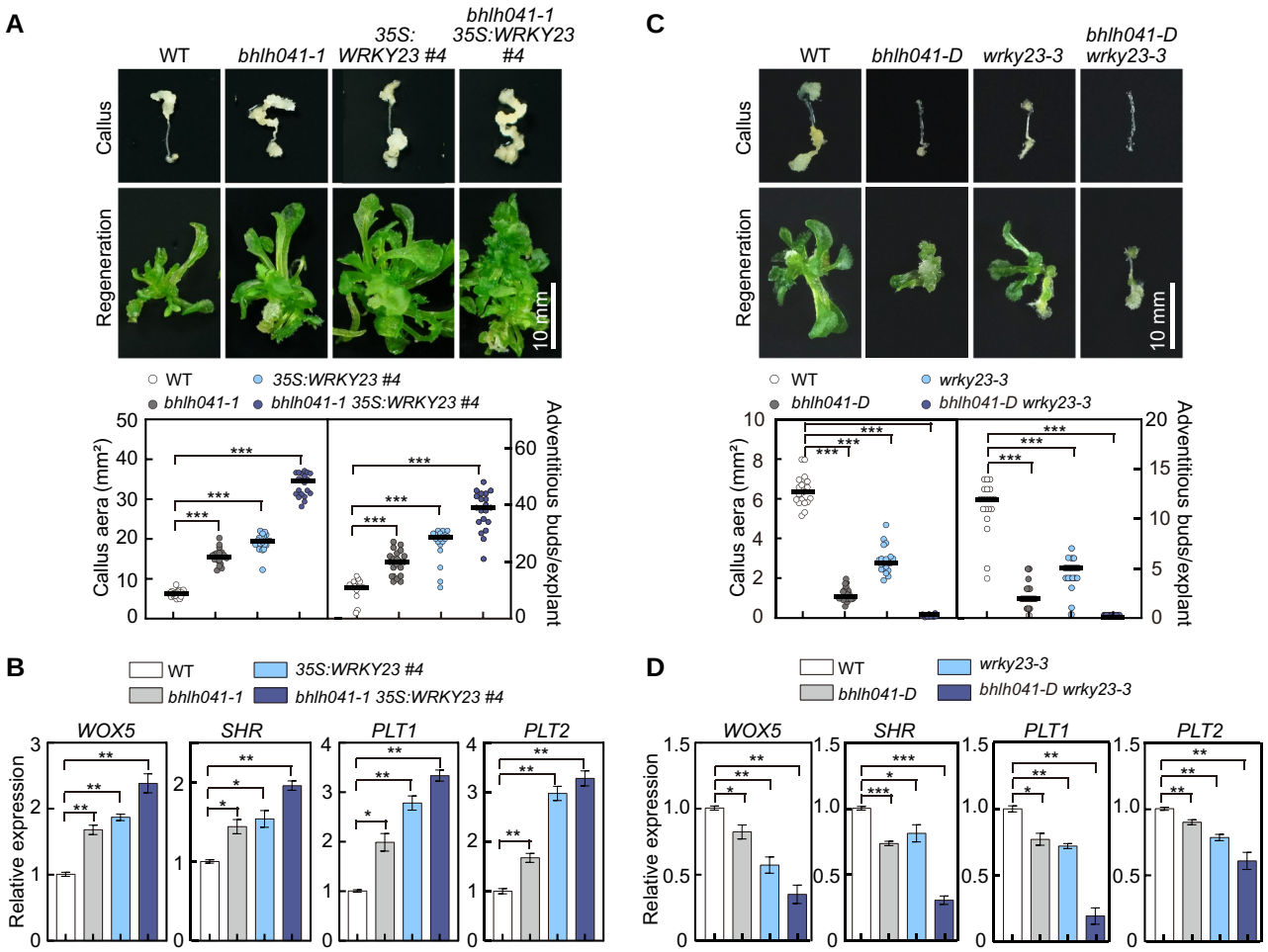

Figure 6. WRKY23 and bHLH041 synergize shoot-regenerating capability of callus. **A)** Callus-forming and shoot-regenerating phenotypes of WT, *bhlh041-1*, *35S:WRKY23*, and *bhlh041-1 35S:WRKY23* root explants and derived calli. **B)** Relative transcript levels of root stem cell genes in root explant-derived callus of the genotypes described in **A)**. **C)** Callus-forming and shoot-regenerating phenotypes of WT, *bhlh041-D*, *wrky23-3*, and *bhlh041-D wrky23-3* root explants and derived calli. **D)** Relative transcript levels of root stem cell genes in root explant-derived callus of the genotypes described in **C)**. The callus area from each root explant on CIM and the number of regenerating shoots from each callus on SIM were determined ($n = 20$ explants) in **A** and **C**, Scale bars, 10 mm. RT-qPCR analysis in **B)** and **D)** was performed with the root explants incubated on CIM for 7 d, and data are shown as means ± SD ($n = 3$ biological replicates). $^*P < 0.05$, $^{**}P < 0.01$, and $^{***}P < 0.001$ by *t*-test.

between these auxin-signaling components and activation of root pluripotent factors during in vitro plant regeneration is unknown. Here, we defined *Arabidopsis* WRKY23 and bHLH041 as a transcriptional activator and repressor, respectively, as being responsible for activation of root stem cell factors to synergize the establishment of callus pluripotency and thus conferring shoot-regenerating capability on callus cells. These findings uncover the transcriptional mechanism underlying the acquisition of cellular pluripotency in auxin-induced callus formation, which links auxin signaling and cellular reprogramming during in vitro plant regeneration. These findings, together with previous works, outline a molecular framework for how callus formation and cellular reprogramming are governed in *Arabidopsis* in vitro regeneration. It is likely that, upon CIM treatment, ARF7- and ARF19-directed LBD accumulation in the pericycle or pericycle-like cells not only triggers the callus-forming program but also leads to the removal of bHLH041, which alleviates the transcriptional repression of *PLT1*, *PLT2*, and *WOX5*. At the same time, auxin-induced WRKY23 downstream of ARF7 and ARF19 directly activates the transcription of *PLT3* and *PLT7*, whose encoded proteins target their downstream genes *PLT1*, *PLT2*, and *WOX5*. The two transcriptional regulatory modules coordinately establish the shoot-regenerating capability of callus cells (Fig. 7).

Intriguingly, WRKY23 directly activates the transcription of *PLT3* and *PLT7* and thus indirectly that of *PLT1*, *PLT2*, and *WOX5*, while the LBD-induced removal of bHLH041 derepresses the transcription of *PLT1*, *PLT2*, and *WOX5*. Indeed, the WOX11–LBD16 module has been shown to promote the acquisition of pluripotency by callus cells via activation of *PLT1* and *PLT2* but not *PLT3*, *PLT5*, or *PLT7* (Liu et al.

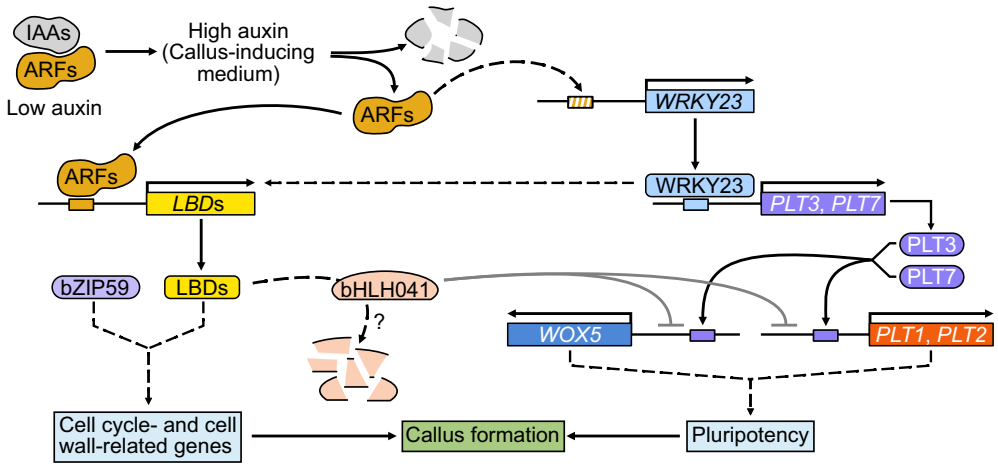

Figure 7. A proposed molecular framework for auxin-induced callus formation. Upon CIM treatment, a high concentration of auxin activates LBDs and WRKY23 via the IAA–ARF7/19 signaling module in the pericycle or pericycle-like cells. LBDs together with their partner bZIP59 trigger callus formation and result in the removal of bHLH041, which alleviates the repression of transcription of *PLT1*, *PLT2*, and *WOX5*. At the same time, WRKY23 directly activates transcription of *PLT3* and *PLT7* and thus indirectly that of their downstream genes *PLT1*, *PLT2*, and *WOX5*. Two transcriptional regulations synergize the callus pluripotency establishment and thus shoot-regenerating capability.

2018). The coexistence and coordination of transcriptional activation and derepression might be a mechanism to ensure that plant somatic cells acquire pluripotency during plant regeneration. WRKY23 is a unique auxin-responsive member of the *Arabidopsis* WRKY family to regulate root development (Grunewald et al. 2008, 2012), while bHLH041 belongs to a large family of bHLH transcription factors present in both plants and animals. It has been shown that different bHLH members function as transcriptional activators or repressors in directing cell fate changes (Toledo-Ortiz et al. 2003). For example, heterodimers of the bHLH factors GhTCE1 and GhTCEE1 promote transcriptional reprogramming during wound-induced callus formation in cotton (*Gossypium hirsutum*) (Deng et al. 2022). In animals, self-renewal, multipotency, and fate choice of neural progenitor cells (NPCs) are controlled by multiple bHLH factors with contradictory functions in promoting NPC proliferation and cell-cycle exit for differentiation (Imayoshi and Kageyama 2014). Importantly, callus formation in in vitro plant regeneration involves both reactivation of cellular mitotic activities and change of cell fates, which are concomitant (Zhao et al. 2001; Williams et al. 2003; Tessadori et al. 2007; Xu et al. 2012). It is likely that the regulatory mechanisms of callus formation and cell fate change are partly shared or overlap. In *Arabidopsis*, auxin-induced LBDs and their partner bZIP59 are sufficient to trigger the formation of pluripotent callus by mediating multiple cellular events, including cell wall metabolism and inhibition of the differentiation program (Fan et al. 2012; Xu, Cao, Xu, et al. 2018; Xu, Cao, Zhang, et al. 2018). Our finding that overexpression or disruption of *bHLH041* also causes callus-forming phenotypes suggests that bHLH041 is involved in LBD-directed cellular mitotic activation. Similarly, although WRKY23 acts in parallel to bHLH041 by targeting *PLT3* and *PLT7*, we also observed that WRKY23 has a regulatory effect on *LBD* transcript levels, suggesting that some extent of crosstalk exists between WRKY23 and LBD-regulated cellular mitotic activity (Fig. 7), which might explain why alteration of WRKY23 results in a callus-forming phenotype.

Although our work defines WRKY23 and bHLH041 as transcriptional activator and repressor to coordinate the establishment of callus pluripotency, the detailed molecular regulations of cellular pluripotency acquisition during auxin-induced callus formation need to be further clarified. First, as LBD transcription factors execute their roles at a transcriptional level, the molecular regulation behind LBD-induced removal of bHLH041 remains unclear. We speculate that other factors are involved in LBD-regulated bHLH041 stability in the forming callus. We also noticed that CIM treatment leads to a decrease in bHLH041 accumulation in other somatic cells besides the pericycle and pericycle-like cells; the biochemical or molecular regulation of bHLH041 stability in these cells needs to be further investigated. Second, we only characterized here how *PLTs* and *WOX5* are regulated by WRKY23 and bHLH041, but we also observed that the transcript levels of *SHR* are regulated by WRKY23 and bHLH041 (Fig. 3). As the regulatory relationship of the PLT–WOX5 and SHR–SCR modules in root stem cell maintenance is not fully defined, how WRKY23 and bHLH041 regulate *SHR* and/or *SCR* remains to be elucidated. Furthermore, auxin-induced callus formation represents a type of cellular reprogramming in plant regeneration, during which genome-wide modifications, such as chromatin reorganization, heterochromatin redistribution, and epigenetic modification occur during the callus formation program (Ikeuchi et al. 2013). How WRKY23- and bHLH041-mediated transcriptional regulations are incorporated with these genome-wide modifications would be

interesting. In addition, since WRKY23 and bHLH041 as well as the root stem cell factors are all transcription factors functioning in nuclei, whether they interact with any of these root stem cell factors remains unclear. It is also possible that some might function in a protein complex during the establishment and maintenance of callus pluripotency. Therefore, further work on these proteins will be helpful to understand the molecular basis of cellular reprogramming in in vitro plant regeneration.

Finally, as both WRKY23 and bHLH041 are involved in regulation of callus formation and shoot regeneration capability, it is likely that appropriate manipulation of their orthologs will be potential to improve the regeneration efficiency of crops and horticultural plants. Therefore, it is worth identifying the orthologs of WRKY23 and bHLH041 to clarify whether such molecular regulations by WRKY23 and bHLH041 are conserved in other plant species, which would benefit plant regeneration-based gene-editing and biotechnological practices.

Materials and methods

Plant materials and growth conditions

The *Arabidopsis* (*A. thaliana*) accession Col-0 was used as a WT and for all transgenic lines. The T-DNA insertion mutants *bhlh041-1* (SAIL_330_F04), *bhlh041-D* (SAIL_258_C03), *lbd16-2* (SALK_040739) (Fan et al. 2012), *air1-2* (SALK_024459c) (Xu, Cao, Zhang, et al. 2018), *plt3* (SALK_127417) (Kareem et al. 2015), and *plt7* (SAIL_1167_C10) (Kareem et al. 2015) were obtained from the ABRC and verified by PCR analyses. The *ProWOX5:GFP-ER* and *ProPLT1:PLT1-YFP* marker lines and *arf7 arf19* double mutant were described previously (Aida et al. 2004; Haecker et al. 2004; Fan et al. 2012). All seeds were surface-sterilized in 1% (w/v) sodium hypochlorite, rinsed 3 times with sterile water, and germinated on half-strength of MS medium (MS powder Coolaber, Beijing, China, 1% [w/v] sucrose, 0.55% [w/v] plant agar, and pH 5.7) at 22 ± 2 °C under long-day conditions (16-h light/8-h dark photoperiod) with incandescent lamps (spectrum: 400 to 700 nm; illumination intensity: 80 to 90 μmol $m^{-2}s^{-1}$); 7-d-old seedlings were transferred to soil and grown in a greenhouse under the same conditions.

Callus induction and shoot regeneration

For characterization of callus formation, cotyledon and root explants of 7-d-old seedlings were incubated on CIM (B5 medium [Coolaber, Beijing, China] supplemented with 2% [w/v] glucose, 0.5 g L^{-1} MES, 2.2 μM 2,4-dichlorophenoxyacetic acid [2,4-D], 0.2 μM kinetin, 0.25% [w/v] phytagel, and pH 5.7) as described (Che et al. 2006) for 21 d, and the formed callus was photographed, and callus area for each explant was quantified with ImageJ software (Shang et al. 2016). For examination of shoot regeneration from callus, the explants incubated on CIM for 7 d with forming callus were transferred onto SIM (MS medium [Coolaber, Beijing, China] supplemented with 1% [w/v] sucrose, 0.5 g L^{-1} MES, 0.25% [w/v] phytagel, 5.0 μM isopentenyladenine and 0.9 μM indole-3-acetic acid [IAA], and pH 5.7) (Che et al. 2006), and the leafy shoots produced from each callus were counted and photographed under a stereomicroscope at 14 d. To monitor transcript abundance of root stem cell marker genes, the root explants incubated CIM for 7 d were collected for RNA isolation, and 5-d-old seedlings harboring a *ProPLT1:PLT1-YFP* or *ProWOX5:GFP-ER* construct were incubated on CIM for 4 d for determination of GFP fluorescent signals. All experiments above were carried out by at least 3 independent biological replicates with more than 20 plants each time.

Plasmid construction and *Arabidopsis* transformation

For generation of the *ProWRKY23:gWRKY23-GFP*, *ProbHLH041:bHLH041-GFP*, and *ProARF7:ARF7-GFP* constructs, a genomic *WRKY23* fragment consisting of a 4,983-bp promoter fragment and a 1,399-bp coding region segment, a *bHLH041* fragment with 2,025 bp of promoter and 1,578 bp of coding region, and *ARF7* fragments with 2,489 bp of promoter and 3,498 bp of coding region fused in-frame and upstream of the *GFP* sequence were cloned into the pCAMBIA1300 vector by the multi-one-step seamless cloning approach, respectively. A 6-glycine linker sequence was inserted upstream of the GFP tag to minimize the influence of the tag on the fusion protein and optimize the stability of the target protein (Robinson and Sauer 1998; Funakoshi and Hochstrasser 2009). The full-length coding sequences of *WRKY23* and *bHLH041* were cloned into the pSuper1300 vector (Chinnusamy et al. 2003), to generate the *35S:WRKY23* and *35S:bHLH041* constructs, respectively. The full-length coding sequences of *LBD16* and *LBD29* were cloned into the pVIP96 vector to generate the *35S:LBD16* and *35S:LBD29* constructs, respectively (Hu et al. 2003). The coding sequence of *WRKY23* was also cloned into the pER10 vector for generating the chemically inducible *ProXVE:WRKY23* construct (Zuo et al. 2000). The primers used for the constructs are listed in Supplemental Data Set S1. All plasmids were verified by Sanger sequencing and introduced into *Agrobacterium* (*Agrobacterium tumefaciens*) strain EHA105 or ABI and transformed into *Arabidopsis* using the floral dip method (Clough and Bent 1998). At least 10 independent transgenic lines with a single T-DNA insertion were generated for each construct, and at least 3 lines of the T3 homozygotes were used for experimental examination.

CRISPR/Cas9 gene editing

To create the *wrky23* allelic mutants, an *Arabidopsis* egg cell-specific promoter-controlled CRISPR/Cas9 gene-editing system was used as previously described (Wang et al. 2015). Briefly, the specific primers containing the 23-bp sequences with 2 PAM sites (5′-N20NGG-3′) corresponding to simple guide RNAs (sgRNAs) were manually designed against the first exon of *WRKY23* and then checked by BLAST for evaluating their specificities on the TAIR website (https://www.arabidopsis.org/Blast/index.jsp). The pCBC-DT1T2 plasmid was used as a template to perform PCR amplification of

the sgRNA sequences. The PCR products were cloned into the pHEE401 vector and introduced into *Arabidopsis* via the floral dipping method as above. The genomic fragments covering the mutation sites from the T1 and T2 transgenic plants were amplified by PCR and sequenced, and homozygous T3 plants without the editing vector were used for characterization. All primers used for generation of the constructs are listed in Supplemental Data Set S1.

Total RNA isolation and gene expression analysis

Total RNAs were isolated using an E.Z.N.A. Plant RNA Kit (OMEGA BioTek) according to the manufacturer's instructions. First-strand cDNA was synthesized with TransScript II All-in-One First-Strand cDNA Synthesis SuperMix (Invitrogen). qPCR was conducted with a SYBR Premix Ex Taq II kit (Takara, Dalian, China) as described previously (Fan et al. 2012), the amplified *ACTIN2* transcript abundance was used as a normalization control, and the relative expression values were calculated using a modified $2^{-\Delta\Delta CT}$ method (Livak and Schmittgen 2001). For RT-PCR analysis, the transcript abundance of *GLYCERALDEHYDE-3-PHOSPHATE DEHYDROGENASE C SUBUNIT 1* (*GAPC*) was used as an internal control. All RT-qPCR and RT-PCR analyses were performed with 3 independent biological replicates. The primers used are listed in Supplemental Data Set S1.

Protein extraction and immunoblotting

To monitor WRKY23 and bHLH041 accumulation during callus induction, total proteins from transgenic *ProWRKY23:gWRKY23-GFP* and *ProbHLH041:bHLH041-GFP* seedlings incubated on CIM for the indicated times were extracted with a Plant Total Protein Extraction Kit (Cwbio, Beijing, China), according to the manufacturer's instructions. The proteins were separated by a 12% SDS-PAGE and immobilized onto nitrocellulose membranes, and immunoblotting was performed with anti-GFP (MBL, lot: M048-3) (1:5000) and anti-ACTIN (EASYBIO, lot: 80790722) (1:5000) primary antibodies followed by horseradish peroxidase-labeled secondary antibody (Bioeasy) (1:10000) and subsequently detected with an ECL Super Sensitive Kit (DiNing). The immunoblotting signals were scanned with a Tanon5200 imaging system.

Confocal microscopy

To visualize accumulation of WRKY23-GFP, bHLH041-GFP, and root meristem markers, 5-d-old seedlings harboring a specific construct or marker incubated on CIM or infiltrated *N. benthamiana* leaves were mounted in 10 mg L^{-1} propidium iodide (Sigma) or distilled water, respectively, and GFP images were collected under an Olympus FV1000-MPE laser scanning microscope. The GFP signal was excited at 488 nm, and the emission was acquired between 500 and 550 nm. The propidium iodide signal was visualized by excitation with an argon laser at 488 nm and detected with a spectral detector set at >585 nm for emission. The GFP fluorescent signals of root stem cell marker lines were determined with the parameters at laser transmissivity: 80%, photomultiplier tube Voltage: 490 V, pinhole: 125 μm, objective lens magnification: 20×. The GFP-positive loci in each image were quantified with ImageJ software.

ChIP-qPCR assay

About 1 g of 10-d-old WT and transgenic seedlings harboring the respective GFP-fusion construct or seedlings incubated in liquid CIM for 12 or 48 h were cross-linked in 1% (w/v) formaldehyde, and the ChIP-qPCR assay was performed as described previously (Bowler et al. 2004), with minor modifications. Briefly, anti-GFP mAb-agarose (MBL) beads were used to immunoprecipitate the protein-DNA complex, and the precipitated DNA was purified for qPCR analysis. The isolated chromatin before precipitation was used as input control. Primers used for ChIP-qPCR are listed in Supplemental Data Set S1. The ChIP-qPCRs were performed with 3 biological and technical replicates.

Transient transcriptional activity assay

The promoter fragments of *WRKY23* (4,983 bp), *PLT3* (3,919 bp), *PLT7* (5,154 bp), *PLT1* (5,611 bp), *PLT2* (5,315 bp), or *WOX5* (4,534 bp) upstream of each translation start site were respectively amplified by PCR from Col-0 genomic DNA and cloned upstream of *LUC* into the TQ379 vector (Zhang et al. 2017), which harbors the *Pro35S:REN* (*Renilla* luciferase) cassette, to create the reporter constructs *ProWRKY23:LUC*, *ProPLT3:LUC*, *ProPLT7:LUC*, *ProPLT1:LUC*, *ProPLT2:LUC*, and *ProWOX5:LUC*, respectively. The full-length coding sequences of *ARF7*, *WRKY23*, and *bHLH041* fused with a 6-glycine linker were respectively cloned upstream of the GFP sequence into p326-35S-cGFP vector with a Ω translational enhancer as effectors (Lin et al. 2016). The Ω translational enhancer (Gallie et al. 1989; Gallie and Kado 1989) was cloned upstream of *ARF7*, *WRKY23*, and *bHLH041* to increase their final expression levels. All primers used for the generation of the constructs are listed in Supplemental Data Set S1.

Three-week-old *Arabidopsis* (Col-0) leaves were used for preparing protoplasts according to a published protocol (Yoo et al. 2007) for dual-luciferase reporter assays. The transfected protoplasts were cultured at 22 °C in the light for 4 h and then in the dark for 14 h. The protoplasts were then lysed with passive lysis buffer (Promega; E1910), and LUC and REN activities were quantified and measured with a luminometer (Promega GloMax Multi Jr). The relative LUC activity was calculated by normalizing to that of REN in 3 biological triplicates.

N. benthamiana infiltration

The full-length coding sequences of *LBD16*, *LBD29*, and *WRKY23* were cloned into the binary vector pSuper1300-FLAG vector, and the full-length coding sequence of *bHLH041* was cloned into the vector pSuper1300-GFP to generate *LBD16-FLAG*, *LBD29-FLAG*, *WRKY23-FLAG*, and *bHLH041-GFP* constructs, respectively. A 6-glycine linker sequence was also inserted upstream of FLAG or GFP tags, and all primers used for

constructions are listed in Supplemental Data Set S1. *Agrobacterium* strain EHA105 harboring the different constructs cultured at 28 °C for 2 d was harvested by centrifugation at 3,500 rpm for 10 min at room temperature and resuspended in infiltration buffer (10 mM MES, 10 mM $MgCl_2$, 150 μM acetosyringone, and pH 5.8) at a final OD600 = 1.0, and then mixed by the specific combination (v:v = 1:1) after 4 h. The mixed *Agrobacterium* cells were infiltrated into the leaves of 4-wk-old *N. benthamiana* plants using an injector as previously described (Sparkes et al. 2006). The fluorescent signals were examined under an Olympus FV1000-MPE laser scanning microscope after plants were kept in dark for 24 h and then in the light for 72 h. The signals were quantified by ImageJ software from 3 biological replicates.

Statistical analysis

All analyses were performed using GraphPad Prism v.8. Statistical analyses were performed using unpaired Student's *t*-test with Welch's correction (not assuming equal standard deviations) (*$P < 0.05$; **$P < 0.01$; ***$P < 0.001$). The values for *N* and the specific statistical test performed for each experiment are described in the figure legends and Supplemental Data Set S2.

Accession numbers

Sequence data in this article can be found in the Arabidopsis Genome initiative or GenBank/EMBL databases under the following accession numbers: *WRKY23* (At2g47260), *PLT1* (At3g20840), *PLT2* (At1g51190), *PLT3* (At5g10510), *PLT5* (At5g57390), *PLT7* (At5g65510), *WOX5* (At3g11260), *SHR* (At4g37650), *ARF7* (At5g20730), *ARF19* (At1g19220), *LBD16* (At2g42430), *LBD29* (At3g58190), *bZIP59* (At2g31370), *bHLH041* (At5g56960), *ACTIN2* (At3g18780), *GPAC* (At3g04120), and *UBQ10* (At4g05320).

Acknowledgments

We are grateful to Drs Ben Scheres, Jim Haseloff, Nam-Hai Chua, Jia-Wei Wang, and Jingbo Jin for providing seeds or constructs used in this study. We acknowledge Huichao Liu and Kezhen Yang for help in preparing some plant samples and the solutions for the ChIP-qPCR experiment.

Author contributions

Y.H. conceived the project; C.X. and Y.H. designed the experiments; C.X. performed most of the experiments; P.C., S.G., X.Y., X.L., B.S., D.Y., and W.X. contributed to the generation of constructs or transgenic *Arabidopsis* plants; and C.X. and Y.H. analyzed data and wrote the manuscript.

Supplemental data

The following materials are available in the online version of this article.

The following materials are available in the online version of this article.

Supplemental Figure S1. Reponses of WRKY23 and bHLH041 to CIM.

Supplemental Figure S2. Characterization of *wrky23* and *35S:WRKY23* plants.

Supplemental Figure S3. Characterization of *bhlh041-1*, *bhlh041-D*, and *35S:bHLH041* plants.

Supplemental Figure S4. Relative *ARF7* and *ARF19* transcript levels in response to CIM and inter-regulation of *WRKY23* and *LBD*s.

Supplemental Figure S5. Genetic interactions of *WRKY23*, *ARF7*, *ARF19*, and *PLT*s.

Supplemental Figure S6. Accumulation of bHLH041 in *arf7 arf19* and *35S:LBD29* plants.

Supplemental Data Set S1. Primers used in this study.

Supplemental Data Set S2. Summary of statistical analyses.

Funding

This work was supported by the Key Program of National Natural Science Foundation of China (grant no. 31830055) and the General Program of National natural Science Foundation of China (grant no. 32170317) and the Strategic Priority Research Program of Chinese Academy of Sciences (grant no. XDB27030102).

Conflict of interest statement. None declared.

Data availability

The data underlying this article are available in the article and in its online supplementary material.

References

Aida M, Beis D, Heidstra R, Willemsen V, Blilou I, Galinha C, Nussaume L, Noh YS, Amasino R, Scheres B. The *PLETHORA* genes mediate patterning of the *Arabidopsis* root stem cell niche. Cell 2004:**119**(1):109–120. https://doi.org/10.1016/j.cell.2004.09.018

Atta R, Laurens L, Boucheron-Dubuisson E, Guivarc'h A, Carnero E, Giraudat-Pautot V, Rech P, Chriqui D. Pluripotency of *Arabidopsis* xylem pericycle underlies shoot regeneration from root and hypocotyl explants grown in vitro. Plant J. 2009:**57**(4):626–644. https://doi.org/10.1111/j.1365-313X.2008.03715.x

Birnbaum KD, Sanchez Alvarado A. Slicing across kingdoms: regeneration in plants and animals. Cell 2008:**132**(4):697–710. https://doi.org/10.1016/j.cell.2008.01.040

Bowler C, Benvenuto G, Laflamme P, Molino D, Probst AV, Tariq M, Paszkowski J. Chromatin techniques for plant cells. Plant J. 2004:**39**(5):776–789. https://doi.org/10.1111/j.1365-313X.2004.02169.x

Che P, Gingerich DJ, Lall S, Howell SH. Global and hormone-induced gene expression changes during shoot development in *Arabidopsis*. Plant Cell 2002:**14**(11):2771–2785. https://doi.org/10.1105/tpc.006668

Che P, Lall S, Howell SH. Developmental steps in acquiring competence for shoot development in *Arabidopsis* tissue culture. Planta 2007:**226**(5):1183–1194. https://doi.org/10.1007/s00425-007-0565-4

Che P, Lall S, Nettleton D, Howell SH. Gene expression programs during shoot, root, and callus development in *Arabidopsis* tissue culture.

Plant Physiol. 2006:**141**(2):620–637. https://doi.org/10.1104/pp.106.081240

Chinnusamy V, Ohta M, Kanrar S, Lee BH, Hong X, Agarwal M, Zhu JK. ICE1: a regulator of cold-induced transcriptome and freezing tolerance in *Arabidopsis*. Genes Dev. 2003:**17**(8):1043–1054. https://doi.org/10.1101/gad.1077503

Clough SJ, Bent AF. Floral dip: a simplified method for *Agrobacterium*-mediated transformation of *Arabidopsis thaliana*. Plant J. 1998:**16**(6):735–743. https://doi.org/10.1046/j.1365-313x.1998.00343.x

Deng J, Sun W, Zhang B, Sun S, Xia L, Miao Y, He L, Lindsey K, Yang X, Zhang X. GhTCE1-GhTCEE1 dimers regulate transcriptional reprogramming during wound-induced callus formation in cotton. Plant Cell 2022:**34**(11):4554–4568. https://doi.org/10.1093/plcell/koac252

Duclercq J, Sangwan-Norreel B, Catterou M, Sangwan RS. De novo shoot organogenesis: from art to science. Trends Plant Sci. 2011:**16**(11):597–606. https://doi.org/10.1016/j.tplants.2011.08.004

Fan M, Xu C, Xu K, Hu Y. LATERAL ORGAN BOUNDARIES DOMAIN transcription factors direct callus formation in *Arabidopsis* regeneration. Cell Res. 2012:**22**(7):1169–1180. https://doi.org/10.1038/cr.2012.63

Fukaki H, Nakao Y, Okushima Y, Theologis A, Tasaka M. Tissue-specific expression of stabilized SOLITARY-ROOT/IAA14 alters lateral root development in *Arabidopsis*. Plant J. 2005:**44**(3):382–395. https://doi.org/10.1111/j.1365-313X.2005.02537.x

Fukaki H, Tameda S, Masuda H, Tasaka M. Lateral root formation is blocked by a gain-of-function mutation in the *SOLITARY-ROOT/IAA14* gene of *Arabidopsis*. Plant J. 2002:**29**(2):153–168. https://doi.org/10.1046/j.0960-7412.2001.01201.x

Funakoshi M, Hochstrasser M. Small epitope-linker modules for PCR-based C-terminal tagging in *Saccharomyces cerevisiae*. Yeast 2009:**26**(3):185–192. https://doi.org/10.1002/yea.1658

Gallie DR, Kado CI. A translational enhancer derived from tobacco mosaic virus is functionally equivalent to a Shine-Dalgarno sequence. Proc Natl Acad Sci U S A. 1989:**86**(1):129–132. https://doi.org/10.1073/pnas.86.1.129

Gallie DR, Lucas WJ, Walbot V. Visualizing mRNA expression in plant protoplasts: factors influencing efficient mRNA uptake and translation. Plant Cell 1989:**1**(3):301–311. https://doi.org/10.1105/tpc.1.3.301

Goh T, Kasahara H, Mimura T, Kamiya Y, Fukaki H. Multiple AUX/IAA-ARF modules regulate lateral root formation: the role of *Arabidopsis* SHY2/IAA3-mediated auxin signalling. Philos Trans R Soc Lond B Biol Sci. 2012:**367**(1595):1461–1468. https://doi.org/10.1098/rstb.2011.0232

Gordon SP, Heisler MG, Reddy GV, Ohno C, Das P, Meyerowitz EM. Pattern formation during de novo assembly of the *Arabidopsis* shoot meristem. Development 2007:**134**(19):3539–3548. https://doi.org/10.1242/dev.010298

Grunewald W, De Smet I, Lewis DR, Löfke C, Jansen L, Goeminne G, Vanden Bossche R, Karimi M, De Rybel B, Vanholme B, et al. Transcription factor WRKY23 assists auxin distribution patterns during *Arabidopsis* root development through local control on flavonol biosynthesis. Proc Natl Acad Sci U S A. 2012:**109**(5):1554–1559. https://doi.org/10.1073/pnas.1121134109

Grunewald W, Karimi M, Wieczorek K, Van de Cappelle E, Wischnitzki E, Grundler F, Inzé D, Beeckman T, Gheysen G. A role for AtWRKY23 in feeding site establishment of plant-parasitic nematodes. Plant Physiol. 2008:**148**(1):358–368. https://doi.org/10.1104/pp.108.119131

Haecker A, Gross-Hardt R, Geiges B, Sarkar A, Breuninger H, Herrmann M, Laux T. Expression dynamics of *WOX* genes mark cell fate decisions during early embryonic patterning in *Arabidopsis thaliana*. Development 2004:**131**(3):657–668. https://doi.org/10.1242/dev.00963

Hu Y, Xie Q, Chua NH. The *Arabidopsis* auxin-inducible gene *ARGOS* controls lateral organ size. Plant Cell 2003:**15**(9):1951–1961. https://doi.org/10.1105/tpc.013557

Ikeuchi M, Sugimoto K, Iwase A. Plant callus: mechanisms of induction and repression. Plant Cell 2013:**25**(9):3159–3173. https://doi.org/10.1105/tpc.113.116053

Imayoshi I, Kageyama R. bHLH factors in self-renewal, multipotency, and fate choice of neural progenitor cells. Neuron 2014:**82**(1):9–23. https://doi.org/10.1016/j.neuron.2014.03.018

Kareem A, Durgaprasad K, Sugimoto K, Du Y, Pulianmackal AJ, Trivedi ZB, Abhayadev PV, Pinon V, Meyerowitz EM, Scheres B, et al. *PLETHORA* Genes control regeneration by a two-step mechanism. Curr Biol. 2015:**25**(8):1017–1030. https://doi.org/10.1016/j.cub.2015.02.022

Kim JY, Yang W, Forner J, Lohmann JU, Noh B, Noh YS. Epigenetic reprogramming by histone acetyltransferase HAG1/AtGCN5 is required for pluripotency acquisition in *Arabidopsis*. EMBO J. 2018:**37**(20):e98726. https://doi.org/10.15252/embj.201798726

Lavy M, Estelle M. Mechanisms of auxin signaling. Development 2016:**143**(18):3226–3229. https://doi.org/10.1242/dev.131870

Lee HW, Cho C, Kim J. Lateral organ boundaries domain16 and 18 act downstream of the AUXIN1 and LIKE-AUXIN3 auxin influx carriers to control lateral root development in *Arabidopsis*. Plant Physiol. 2015:**168**(4):1792–1806. https://doi.org/10.1104/pp.15.00578

Lee HW, Kang NY, Pandey SK, Cho C, Lee SH, Kim J. Dimerization in LBD16 and LBD18 transcription factors is critical for lateral root formation. Plant Physiol. 2017:**174**(1):301–311. https://doi.org/10.1104/pp.17.00013

Lee HW, Kim MJ, Kim NY, Lee SH, Kim J. LBD18 acts as a transcriptional activator that directly binds to the *EXPANSIN14* promoter in promoting lateral root emergence of *Arabidopsis*. Plant J. 2013:**73**(2):212–224. https://doi.org/10.1111/tpj.12013

Lee HW, Kim NY, Lee DJ, Kim J. LBD18/ASL20 regulates lateral root formation in combination with LBD16/ASL18 downstream of ARF7 and ARF19 in *Arabidopsis*. Plant Physiol. 2009:**151**(3):1377–1389. https://doi.org/10.1104/pp.109.143685

Lee K, Park OS, Seo PJ. *Arabidopsis* ATXR2 deposits H3K36me3 at the promoters of *LBD* genes to facilitate cellular dedifferentiation. Sci Signal. 2017:**10**(507):eaan0316. https://doi.org/10.1126/scisignal.aan0316

Lin XL, Niu D, Hu ZL, Kim DH, Jin YH, Cai B, Liu P, Miura K, Yun DJ, Kim WY, et al. An *Arabidopsis* SUMO E3 ligase, SIZ1, negatively regulates photomorphogenesis by promoting COP1 activity. PLoS Genet. 2016:**12**(4):e1006016. https://doi.org/10.1371/journal.pgen.1006016

Liu J, Hu X, Qin P, Prasad K, Hu Y, Xu L. The WOX11-LBD16 pathway promotes pluripotency acquisition in callus cells during de novo shoot regeneration in tissue culture. Plant Cell Physiol. 2018:**59**(4):734–743. https://doi.org/10.1093/pcp/pcy010

Livak KJ, Schmittgen TD. Analysis of relative gene expression data using real-time quantitative PCR and the 2(-Delta Delta C(T)) method. Methods 2001:**25**(4):402–408. https://doi.org/10.1006/meth.2001.1262

Okushima Y, Fukaki H, Onoda M, Theologis A, Tasaka M. ARF7 and ARF19 regulate lateral root formation via direct activation of *LBD/ASL* genes in *Arabidopsis*. Plant Cell 2007:**19**(1):118–130. https://doi.org/10.1105/tpc.106.047761

Powers SK, Holehouse AS, Korasick DA, Schreiber KH, Clark NM, Jing H, Emenecker R, Han S, Tycksen E, Hwang I, et al. Nucleo-cytoplasmic partitioning of ARF proteins controls auxin responses in *Arabidopsis thaliana*. Mol Cell. 2019:**76**(1):177–190.e175. https://doi.org/10.1016/j.molcel.2019.06.044

Prát T, Hajný J, Grunewald W, Vasileva M, Molnár G, Tejos R, Schmid M, Sauer M, Friml J. WRKY23 Is a component of the transcriptional network mediating auxin feedback on PIN polarity. PLoS Genet. 2018:**14**(1):e1007177. https://doi.org/10.1371/journal.pgen.1007177

Radhakrishnan D, Kareem A, Durgaprasad K, Sreeraj E, Sugimoto K, Prasad K. Shoot regeneration: a journey from acquisition of competence to completion. Curr Opin Plant Biol. 2018:**41**:23–31. https://doi.org/10.1016/j.pbi.2017.08.001

Robinson CR, Sauer RT. Optimizing the stability of single-chain proteins by linker length and composition mutagenesis. Proc Natl Acad Sci U S A. 1998:**95**(11):5929–5934. https://doi.org/10.1073/pnas.95.11.5929

Shang B, Xu C, Zhang X, Cao H, Xin W, Hu Y. Very-long-chain fatty acids restrict regeneration capacity by confining pericycle competence for callus formation in *Arabidopsis*. Proc Natl Acad Sci U S A. 2016:**113**(18):5101–5106. https://doi.org/10.1073/pnas.1522466113

Skoog F, Miller CO. Chemical regulation of growth and organ formation in plant tissues cultured in vitro. Symp Soc Exp Biol. 1957:**54**(11):118–130.

Sparkes IA, Runions J, Kearns A, Hawes C. Rapid, transient expression of fluorescent fusion proteins in tobacco plants and generation of stably transformed plants. Nat Protoc. 2006:**1**(4):2019–2025. https://doi.org/10.1038/nprot.2006.286

Sugimoto K, Gordon SP, Meyerowitz EM. Regeneration in plants and animals: dedifferentiation, transdifferentiation, or just differentiation? Trends Cell Biol. 2011:**21**(4):212–218. https://doi.org/10.1016/j.tcb.2010.12.004

Sugimoto K, Jiao Y, Meyerowitz EM. *Arabidopsis* regeneration from multiple tissues occurs via a root development pathway. Dev Cell. 2010:**18**(3):463–471. https://doi.org/10.1016/j.devcel.2010.02.004

Sugiyama M. Partnership for callusing. Nat Plants. 2018:**4**(2):69–70. https://doi.org/10.1038/s41477-018-0104-2

Tatematsu K, Kumagai S, Muto H, Sato A, Watahiki MK, Harper RM, Liscum E, Yamamoto KT. *MASSUGU2* encodes Aux/IAA19, an auxin-regulated protein that functions together with the transcriptional activator NPH4/ARF7 to regulate differential growth responses of hypocotyl and formation of lateral roots in *Arabidopsis thaliana*. Plant Cell 2004:**16**(2):379–393. https://doi.org/10.1105/tpc.018630

Tessadori F, Chupeau MC, Chupeau Y, Knip M, Germann S, van Driel R, Fransz P, Gaudin V. Large-scale dissociation and sequential reassembly of pericentric heterochromatin in dedifferentiated *Arabidopsis* cells. J Cell Sci. 2007:**120**(Pt 7):1200–1208. https://doi.org/10.1242/jcs.000026

Tian Q, Reed JW. Control of auxin-regulated root development by the *Arabidopsis thaliana SHY2/IAA3* gene. Development 1999:**126**(4):711–721. https://doi.org/10.1242/dev.126.4.711

Toledo-Ortiz G, Huq E, Quail PH. The *Arabidopsis* basic/helix-loop-helix transcription factor family. Plant Cell 2003:**15**(8):1749–1770. https://doi.org/10.1105/tpc.013839

Uehara T, Okushima Y, Mimura T, Tasaka M, Fukaki H. Domain II mutations in CRANE/IAA18 suppress lateral root formation and affect shoot development in *Arabidopsis thaliana*. Plant Cell Physiol. 2008:**49**(7):1025–1038. https://doi.org/10.1093/pcp/pcn079

Valvekens D, Van Montagu M, Van Lijsebettens M. *Agrobacterium tumefaciens*-mediated transformation of *Arabidopsis thaliana* root explants by using kanamycin selection. Proc Natl Acad Sci U S A. 1988:**85**(15):5536–5540. https://doi.org/10.1073/pnas.85.15.5536

Wang FX, Shang GD, Wang JW. Towards a hierarchical gene regulatory network underlying somatic embryogenesis. Trends Plant Sci. 2022:**27**(12):1209–1217. https://doi.org/10.1016/j.tplants.2022.06.002

Wang S, Tiwari SB, Hagen G, Guilfoyle TJ. AUXIN RESPONSE FACTOR7 restores the expression of auxin-responsive genes in mutant *Arabidopsis* leaf mesophyll protoplasts. Plant Cell 2005:**17**(7):1979–1993. https://doi.org/10.1105/tpc.105.031096

Wang ZP, Xing HL, Dong L, Zhang HY, Han CY, Wang XC, Chen QJ. Egg cell-specific promoter-controlled CRISPR/Cas9 efficiently generates homozygous mutants for multiple target genes in *Arabidopsis* in a single generation. Genome Biol. 2015:**16**(1):144. https://doi.org/10.1186/s13059-015-0715-0

Williams L, Zhao J, Morozova N, Li Y, Avivi Y, Grafi G. Chromatin reorganization accompanying cellular dedifferentiation is associated with modifications of histone H3, redistribution of HP1, and activation of E2F-target genes. Dev Dyn. 2003:**228**(1):113–120. https://doi.org/10.1002/dvdy.10348

Xu C, Cao H, Xu E, Zhang S, Hu Y. Genome-wide identification of *Arabidopsis* LBD29 target genes reveals the molecular events behind auxin-induced cell reprogramming during callus formation. Plant Cell Physiol. 2018:**59**(4):744–755. https://doi.org/10.1093/pcp/pcx168

Xu C, Cao H, Zhang Q, Wang H, Xin W, Xu E, Zhang S, Yu R, Yu D, Hu Y. Control of auxin-induced callus formation by bZIP59-LBD complex in *Arabidopsis* regeneration. Nat Plants. 2018:**4**(2):108–115. https://doi.org/10.1038/s41477-017-0095-4

Xu K, Liu J, Fan M, Xin W, Hu Y, Xu C. A genome-wide transcriptome profiling reveals the early molecular events during callus initiation in *Arabidopsis* multiple organs. Genomics 2012:**100**(2):116–124. https://doi.org/10.1016/j.ygeno.2012.05.013

Yoo SD, Cho YH, Sheen J. *Arabidopsis* mesophyll protoplasts: a versatile cell system for transient gene expression analysis. Nat Protoc. 2007:**2**(7):1565–1572. https://doi.org/10.1038/nprot.2007.199

Zhai N, Pan X, Zeng M, Xu L. Developmental trajectory of pluripotent stem cell establishment in *Arabidopsis* callus guided by a quiescent center-related gene network. Development 2023:**150**(5):dev200879. https://doi.org/10.1242/dev.200879

Zhai N, Xu L. Pluripotency acquisition in the middle cell layer of callus is required for organ regeneration. Nat Plants. 2021:**7**(11):1453–1460. https://doi.org/10.1038/s41477-021-01015-8

Zhang TQ, Lian H, Zhou CM, Xu L, Jiao Y, Wang JW. A two-step model for de novo activation of *WUSCHEL* during plant shoot regeneration. Plant Cell 2017:**29**(5):1073–1087. https://doi.org/10.1105/tpc.16.00863

Zhang S, Yu R, Yu D, Chang P, Guo S, Yang X, Liu X, Xu C, Hu Y. The calcium signaling module CaM-IQM destabilizes IAA-ARF interaction to regulate callus and lateral root formation. Proc Natl Acad Sci U S A. 2022:**119**(27):e2202669119. https://doi.org/10.1073/pnas.2202669119

Zhao J, Morozova N, Williams L, Libs L, Avivi Y, Grafi G. Two phases of chromatin decondensation during dedifferentiation of plant cells: distinction between competence for cell fate switch and a commitment for S phase. J Biol Chem. 2001:**276**(25):22772–22778. https://doi.org/10.1074/jbc.M101756200

Zuo J, Niu QW, Chua NH. An estrogen receptor-based transactivator XVE mediates highly inducible gene expression in transgenic plants. Plant J. 2000:**24**(2):265–273. https://doi.org/10.1046/j.1365-313x.2000.00868.x